

Implementation of Compressive Sensing for Preclinical Cine-MRI

Elliot Tan^a, Ming Yang^b, Lixin Ma^b, Yahong Rosa Zheng^c

^aPrinceton University; ^bUniversity of Missouri, Department of Radiology, Nuclear Science and Engineering Institute, and Harry S. Truman Memorial VA Hospital; ^cMissouri University of Science and Technology, Department of Electrical and Computer Engineering

ABSTRACT

This paper presents a practical implementation of Compressive Sensing (CS) for a preclinical MRI machine to acquire randomly undersampled k-space data in cardiac function imaging applications. First, random undersampling masks were generated based on Gaussian, Cauchy, wrapped Cauchy and von Mises probability distribution functions by the inverse transform method. The best masks for undersampling ratios of 0.3, 0.4 and 0.5 were chosen for animal experimentation, and were programmed into a Bruker Avance III BioSpec 7.0T MRI system through method programming in ParaVision. Three undersampled mouse heart datasets were obtained using a fast low angle shot (FLASH) sequence, along with a control undersampled phantom dataset. ECG and respiratory gating was used to obtain high quality images. After CS reconstructions were applied to all acquired data, resulting images were quantitatively analyzed using the performance metrics of reconstruction error and Structural Similarity Index (SSIM). The comparative analysis indicated that CS reconstructed images from MRI machine undersampled data were indeed comparable to CS reconstructed images from retrospective undersampled data, and that CS techniques are practical in a preclinical setting. The implementation achieved 2 to 4 times acceleration for image acquisition and satisfactory quality of image reconstruction.

Keywords: MRI, compressive sensing, random undersampling, reconstruction, reconstruction error, structural similarity index, mouse heart

1. INTRODUCTION

The low temporal resolution of conventional magnetic resonance imaging (MRI) presents a challenge in many clinical and preclinical applications, especially in detection of diastolic and systolic cardiac dysfunctions. The required temporal resolution in imaging animal models (for example a mouse heart) is even higher than clinical applications because of two major reasons. One is that the mouse heart beats at a much faster rate (~400 beats per minute under anesthesia) than a human heart (~60 beats per minute). The other is that the mouse needs to breathe while in the MRI machine, unlike a human patient who can hold their breath while being scanned. Therefore, improving the speed of MRI scan is critical in these preclinical applications.

Two approaches have been applied to MRI for increasing the imaging speed: parallel imaging and Compressive Sensing (CS). Parallel imaging uses multiple RF coils to acquire multiple k-space lines simultaneously. In contrast, the CS technique exploits the sparsity in MRI images and acquires only a fraction of the k-space lines of the conventional Nyquist sampling rate². Significant research effort has been put in the CS techniques in recent years. However, majority of the works reported in the literature uses retrospective undersampling³. Reports about how a random sampling scheme can be applied on actual MRI systems remain very scarce^{1, 5}. Han et al., 2012 demonstrated a machine-undersampled CS technique on a preclinical dynamic contrast-enhanced (DCE) MRI by modifying a fast low angle shot (FLASH) pulse sequence and incorporating a 3D gradient array. However, this approach presents challenges to mouse cardiac imaging because ECG gating is often required to align the k-space data cube, while applying different undersampling masks at different time points proves to be difficult in cine-MRI¹.

In this work, we tried to implement multiple undersampling masks to cine-MRI. Our approach is to record the heart beat cycles along with the MRI k-space data without using ECG gating. We can then rely on post-processing to align the undersampled

data cube and use 3D CS method to reconstruct the video. Our goal is to achieve less than 1% loss of video quality with at least 4 times acceleration in imaging scan. Our previous work used the retrospective undersampling and 3D CS reconstruction³. This paper reports our preliminary effort towards applying random undersampling on a preclinical Bruker Avance III BioSpec 7.0T MRI machine. Several probability distributions are studied for generating random undersampling masks. Programming of ParaVision method is accomplished to realize actual undersampling on the MRI. Phantom and mouse heart experiments are conducted to demonstrate that the actual undersampling achieves similar results as retrospective undersampling in terms of subjective evaluation and objective evaluations such as reconstruction error and Structural Similarity Index (SSIM).

2. METHOD

Our experimental implementation of CS consisted of four steps:

1. Preprocessing to generate undersampling masks
2. Method Programming in ParaVision software
3. Imaging procedure in animal experiments to acquire machine undersampled data
4. Postprocessing for image reconstruction with CS

The details of the four steps are presented next.

2.1 Pre-processing

To generate incoherent undersampling masks, we selected several probability distribution functions (pdfs) and evaluated the masks through retrospective undersampling and subsequent image reconstructions. The quality of the reconstructed images was measured mean reconstruction error and the Structural Similarity Index (SSIM) against images reconstructed from fully sampled k-space data. The best masks were selected for implementation in animal experiments in step 3.

The pdfs considered were von Mises, wrapped Cauchy, Gaussian and Cauchy. Lustig et al., 2007 suggested using pdfs with diminishing density according to a power of distance from the origin. These four pdfs considered fulfill such a requirement. In theory, wrapped distributions (von Mises, wrapped Cauchy) are mathematically more accurate than the non-wrapped distributions (Gaussian, Cauchy) for discrete k-space sampling. However, simulation evaluations of wrapped pdf generated masks versus non-wrapped pdf generated masks demonstrated that there was no significant difference between wrapped and non-wrapped distributions. Retrospective undersampling results indicated von Mises performed similarly to Gaussian, and wrapped Cauchy performed similarly to Cauchy. Cauchy and wrapped Cauchy produced reconstructed images of slightly less quality than von Mises and Gaussian.

The pdfs of the four distributions are listed as follows:

$$Gaussian : \frac{1}{\sqrt{2\pi\sigma^2}} \exp \left\{ -\frac{(x-\mu)^2}{2\sigma^2} \right\}, \quad \mu - \text{mean}, \quad \sigma^2 - \text{variance}, \quad -\infty < x < \infty \quad (1)$$

$$Cauchy : \frac{1}{\pi\gamma \left[1 + \left(\frac{x-x_0}{\gamma} \right)^2 \right]}, \quad x_0 - \text{mean}, \quad \gamma - \text{concentration}, \quad -\infty < x < \infty \quad (2)$$

$$von Mises : \frac{e^{\kappa \cos(x-\mu)}}{2\pi I_0(\kappa)}, \quad \mu - \text{mean}, \quad \kappa - \text{concentration}, \quad -\pi \leq x \leq \pi \quad (3)$$

$$Wrapped Cauchy : \frac{1}{2\pi} \frac{\sinh(\gamma)}{\cosh(\gamma) - \cos(x-\mu)}, \quad \mu - \text{mean}, \quad \gamma - \text{concentration}, \quad -\pi \leq x \leq \pi \quad (4)$$

where $I_0()$, $\cosh()$, $\sinh()$ are modified Bessel function of order zero, hyperbolic cosine, and hyperbolic sine functions, respectively. The random variables for these distributions were generated by the inverse transform method which maps a uniform random variable into the random variables of the desired pdf. Undersampling masks were then created by scaling the generated random variables to the desired range. For example, the gradient parameter of the MRI system ranges from -1 to 1. The CS reconstruction algorithm discretizes the ky-space into 1-128 or 1-256 with the center value corresponding to the zero gradient. For Gaussian and Cauchy distributions, if some of the generated random variables exceeded the desired ranges, then they were simply discarded. The parameters of concentration, variance and gamma were selected from 1-200, 1-100, and 1-100, respectively for simulation.

Two metrics were used to quantitatively analyze the quality of image reconstruction: reconstruction error (%) and mean Structural Similarity Index (SSIM). They are defined as follows:

$$RE = \frac{\|s - s_0\|_2}{\|s_0\|_2} \quad (5)$$

$$SSIM(s, s_0) = \frac{(2\mu_s\mu_{s_0} + C_1)(2\sigma_{ss_0} + C_2)}{(\mu_s^2 + \mu_{s_0}^2 + C_1)(\sigma_s^2 + \sigma_{s_0}^2 + C_2)} \quad (6)$$

where μ_s and σ_s^2 are the mean and variance of the reconstructed (s), and σ_{ss_0} is the correlation between the reconstructed (s) and the reference image (s_0).

SSIM is considered a metric more consistent with human eye perception when compared to reconstruction error, and has been commonly used for 2D image quality assessment. Wang et al. states that the index separates the task of similarity into the three comparisons of luminance, contrast and structure, while also considering symmetry, boundedness and the unique maximum⁴. Since MRI images are ultimately analyzed by humans, SSIM is perhaps a more robust metric than reconstruction error.

In our simulation, SSIM was calculated with the typical parameter settings: $C_1 = 1 \times 10^{-4}$ and $C_2 = 9 \times 10^{-4}$, and the weighting function was selected as a spherical-symmetric Gaussian lowpass filter of size 16 x 16 x 16 with standard deviation of 4 samples, normalized to a unit sum. If the reconstructed image is exactly the same as the reference image, then SSIM is equal to 1.

The best parameters for all pdfs were determined through simulations of 100 trials of retrospective undersampling. The concentration (von Mises), variance (Gaussian) and gamma (Cauchy, wrapped Cauchy) of each pdf was selected based on the reconstructed image which had the highest SSIM and lowest mean reconstruction error against a reference image in each simulation.

Masks of three different undersampling ratios (0.3, 0.4 and 0.5) were generated. Ratio indicates the number of random variables drawn based on the size of the k-space, e.g. a ratio = 0.1 for a k-space of 256 x 256 meant ~26 ky lines would be selected for sampling. 0.3, 0.4, and 0.5 ratio masks for mouse heart imaging were chosen, along with a 0.3 ratio mask for phantom imaging. The chosen masks produced the best reconstructed images according to SSIM and mean reconstruction error measurements against a reference image.

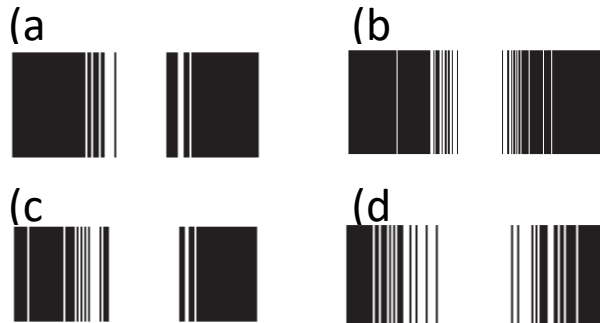
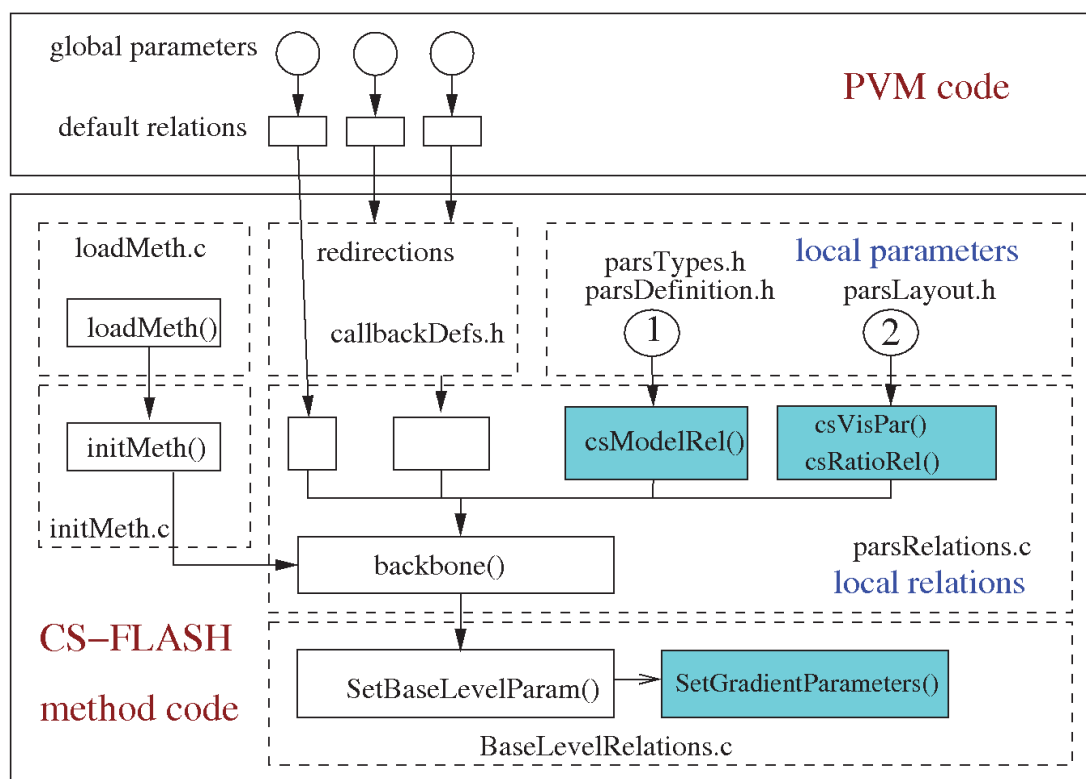


Figure 1. Undersampling masks chosen for animal experimentation. (a) ratio of 0.3 for mouse heart, (c) ratio of 0.4 for mouse heart (b) ratio of 0.3 for phantom (d) ratio of 0.5 for mouse heart. All sampling patterns used Gaussian pdf except (c) which used von Mises.

2.2 Method Programming in ParaVision



First, the variables needed for compressive mode are defined in the three header files and their relations to new functions are defined in `backbone()`. Second, the new functions for compressive mode and the corresponding GUI functions are defined in `parsRelations.c`. Third, the gradient parameters converted from the generated undersampling mask are incorporated in the function `SetBaseLevelParam()` through `SetGradientParameters()`. The image reconstruction was done in MatLab and the `RecoRelations.c` was neither used nor modified. Successful compilation of the source code generates object files and pulse program file `cs_flash.ppg` which are used to control the MRI scan and display a GUI in ParaVision.

3.3 Imaging Procedure

A phantom image was acquired as a control because there is no inherent movement by the phantom, unlike a mouse heart. The phantom is a Bruker MRI Geometry Phantom (Model No. 1PT10681) which was made of a 50 mL centrifuge tube filled with Lego blocks and a mixture of $\text{CuSO}_4 \cdot 2\text{H}_2\text{O}$ (concentration = 1g/L), Agarose (concentration = 10 g/L) and H_2O . The undersampling mask generated for a phantom image in step 1 was used during data acquisition.

Wild type C57BL/6J female mice (The Jackson Laboratory) aged 15 weeks weighing 20 g were imaged with a Bruker Avance III BioSpec 7.0T MRI machine. A quadrature driven birdcage 300 MHz radiofrequency (RF) coil with a 35 mm inner diameter were used. The animal experiments were conducted in accordance with the highest standards of care as outlined in the National Institute of Health guidelines for Care and Use of Laboratory Animals and the Policy and Procedures for Animal Research at the Harry S. Truman Memorial Veterans' Hospital.

The mouse was anesthetized with around 2% isoflurane in oxygen and their heart rates were maintained around 360 beats per minute. The mouse was placed supine in a cradle, and ECG electrodes were inserted into its right forepaw and left rear paw. A respiration sensor was taped on its chest. The cradle was then inserted into the RF coil, which was then placed in the center of the MRI machine. The ECG was used to trigger the MR scan immediately after the R-wave in the cardiac cycle. The body temperature of the mouse was maintained by warm air circulating through the MRI bore. An animal physiological monitoring system was used to monitor the body temperature of the mouse, as well as ECG and respiratory gating.

Scout images at axial, coronal and sagittal planes were used to localize the animal and confirm its positioning in the MRI machine. A multi-slice gradient echo pulse sequence was then applied to obtain three sagittal images across the heart location based on the scout images. These images were used for determining the long-axis (coronal) plane of the left ventricle. The short axis plane was located by positioning the slice perpendicular to the long-axis plane. A fast low angle shot sequence (FLASH) was then applied to collect the ky lines in k-space. The TR (repetition time) was calculated in real time as the RR-delay divided by 16, and the TE (echo time) was 1.57 ms.

For both 128 x 128 and 256 x 256 data sets, a Nyquist sampling data set was acquired in a scan time of 2-3 minutes. After a 1 minute delay, three 2D slices of the mouse heart were then acquired using undersampling masks generated in step 1 with a scan time of ~45 seconds.

MRI scan time can be calculated using the equation:

$$\text{Scan Time} = \text{Matrix Phase Encoding Size} * \text{RR delay} * \text{Number of Excitations} \quad (8)$$

RR delay and the Number of Excitations were constant between experiments. Therefore, the undersampling ratios of 0.3, 0.4 and 0.5 would result in new scan times 0.3, 0.4 and 0.5 times the original scan time.

4.4 Postprocessing: Compressive Sensing reconstruction

The MRI CS Toolbox by Brice Hirst³ was used to reconstruct undersampled data. The toolbox utilizes MATLAB with YALL1 v1.4. The wavelet coiflet5 transform domain was used along with a direct Fourier transform option.

3. RESULTS

Quantitative analysis was done on a control phantom data set (256 x 256), and three mouse heart data sets (128 x 128) acquired with ratios of 0.3, 0.4 and 0.5. Four images were acquired for the phantom data set, as shown in Fig. 3:

1. Image reconstruction of Nyquist sampled data using a direct Fourier transform (DFT), referred to as full image;
2. CS reconstructed image using wavelet coiflet5 domain of machine undersampled data, referred to as undersampled image;
3. Retrospective undersampling image CS reconstructed using wavelet coiflet5 domain, referred to as retrospective image;
4. Image reconstruction of machine undersampled data using a DFT, referred to as DFT image.

Only the first three images were reconstructed for the mouse heart data set and the resulting images are shown in Fig. 4. The DFT images for the mouse heart were omitted because a comparison between the DFT reconstructed phantom image and CS reconstructed phantom image already demonstrated that CS was the advantageous reconstruction technique.

Reconstruction error and SSIM were measured for the retrospective image, undersampled image, and DFT images in reference to the full image. An SSIM was also measured between the machine undersampled CS reconstruction and the retrospective reconstruction in order to quantify the difference between a CS reconstruction in a realistic scenario versus a simulated setting. The results are shown in Table 1.

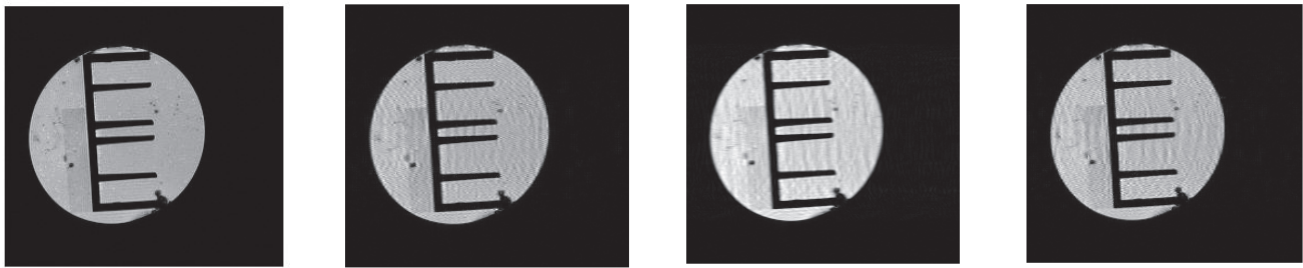


Figure 3. Phantom Data with 72/256 lines sampled using a ratio of 0.3. From left, first is fully sampled image, second is the image reconstruction of machine acquired data, third is the image reconstruction of retrospective undersampling, fourth is a DFT of machine acquired data

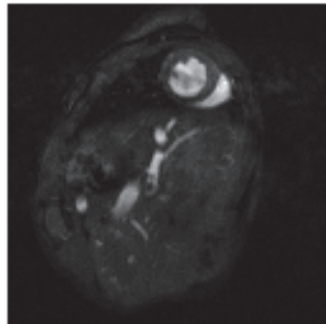


Figure 4. DFT reconstructed Nyquist sampling of the mouse heart.

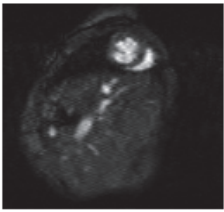
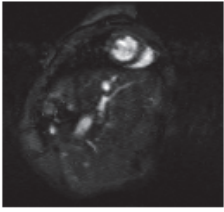
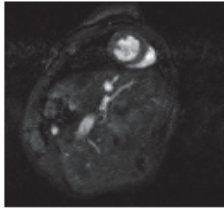
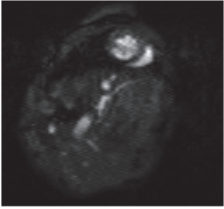
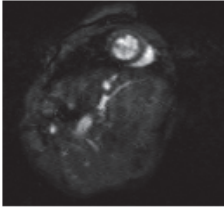
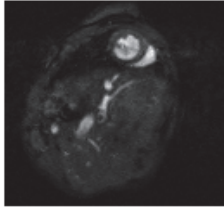
	Ratio = 0.3	Ratio = 0.4	Ratio = 0.5
Undersampled			
Retrospective			

Figure 5. Mouse heart data organized by CS reconstructions from machine undersampled data, retrospective undersampling and direct Fourier transform (DFT) reconstruction from machine undersampled data and undersampling ratios of 0.3, 0.4 and 0.5.

Table 1. SSIM and Reconstruction Error results for phantom and mouse heart images of ratios 0.3, 0.4 and 0.5.

<u>SSIM</u>	Phantom 72/256	Heart 38/128	Heart 52/128	Heart 70/128
Retrospective / Full	0.9705	0.9795	0.9867	0.9929
Undersampled / Full	0.9685	0.9453	0.9390	0.9444
DFT / Full	0.9169	-	-	-
Simulation / undersampled	0.9699	0.9480	0.9378	0.9465

<u>Reconstruction Error (%)</u>	Phantom 72/256	Heart 38/128	Heart 52/128	Heart 70/128
Retrospective / Full	8.14	6.4208	9.5839	3.2734
Undersampled / Full	3.9335	15.5324	12.8025	17.1430
DFT / Full	23.8697	-	-	-

4. DISCUSSION

4.1 Phantom Imaging

The phantom results proved very encouraging. The undersampled image had a higher SSIM ($0.9685 > 0.91699$) and a lower reconstruction error ($3.9335 < 23.8697$) than the DFT image when both images were compared to the full image. This demonstrates that the CS reconstruction technique is more effective than a DFT reconstruction in producing a higher quality image in reference to the Nyquist sampled image. The undersampled image also performed similarly to the retrospective image, with their SSIM measurements in comparison to the full image being very close (0.9705 and 0.9685). The SSIM index of 0.9699 was obtained when comparing these two images to each other indicating that CS reconstruction performs with similar success in both a preclinical setting and a simulated setting for a static phantom source.

Visually, the undersampled image has less aliasing artifacts, borders appear sharper, and the contrast is more accurate when compared to the DFT image. The undersampled image looks very similar to the retrospective image. Compared to the full image, the undersampled image has minor aliasing artifacts, and slightly blurred borders.

4.2 Mouse Heart Imaging

Artifacts were present in the full image of the mouse heart. A band appears horizontally across the opening of the left ventricle due to the blood flowing in and out of the frame during data acquisition. There are also ghost artifacts within and outside of the mouse heart because of the movement of the animal inside the MRI machine. The images selected for analysis were done with respiratory gating in order to alleviate the artifacts caused by the animal's movements. Artifacts were not caused or enhanced by the CS reconstruction itself.

According to the undersampled images, there seems to be no correlation between ratio and image quality for this particular mouse heart image. In theory, higher ratios should generate an image of higher quality due to more ky lines being sampled. However, SSIM measurements indicated that the 0.5 ratio image reconstruction was of the best quality, followed by the 0.3 ratio image reconstruction, with the 0.4 ratio image reconstruction being of the worst quality.

According to retrospective undersampling, SSIM indicates that a higher ratio resulted in a higher SSIM index of their image reconstruction. Reconstruction error indicates similar results to the undersampled ratios.

However, it may be unreasonable to compare the ratio reconstructed images to each other since each data set was collected at a different time. As a result, each ratio reconstructed image will have different distortions due to the varying biological processes of the mouse.

The difference between the retrospective and the undersampled images may be attributed to the time difference of data acquisition. The heart could have been at a slightly different phase in the cardiac cycle during the data acquisition for the full and undersampled images, leading to an enhanced difference. SSIM measurements between the retrospective and undersampled images also indicates that the two images are relatively similar to each other (0.9480, 0.9378, 0.9465), demonstrating that the CS technique is functioning correctly.

Visually, retrospective and undersampled images are of similar quality. It is important to note that all three ratio reconstructed images are of enough quality to be used for further quantitative analysis on the image, specifically on the left ventricle.

4.3 Comparison of phantom and mouse heart imaging

In general, retrospective images of the mouse heart were of higher quality than the retrospective image of the phantom, as indicated by their higher SSIM indices and lower reconstruction error. However, the undersampled phantom image had the

highest SSIM index (0.9685) and lowest reconstruction error (3.9335%) out of all undersampled images acquired. Therefore, in practice, compressive sensing may be more effective when the Nyquist sampling image is of high quality with a reduced amount of artifacts. It seems advantageous to acquire data with a lower noise level to produce an improved CS reconstructed image for mouse heart imaging.

5. CONCLUSION

CS reconstructions of machine undersampled data sets produces images of similar quality to CS reconstructions of retrospective undersampling data. Regardless of undersampling ratio, reconstructed images have enough quality to be utilized for future image processing e.g. determining volume of the left ventricle. Therefore, CS techniques should be implemented in preclinical MRI machines to reduce overall scan time, and from our results the ratio of 0.3 can be used to minimize scan time.

Future work can be done by generating a cine data set where each frame is undersampling with a different mask. As a result, the sparsity in the time domain can be exploited, and perhaps the CS reconstruction technique on cine mouse heart imaging will be more effective. Additionally, different phases of the cardiac cycle can be imaged and analyzed.

ACKNOWLEDGEMENTS

Special thanks are due to Brice Hirst, who provided the MATLAB code for the MRI CS Toolbox. This work was financially supported by the University of Missouri Research Board Fund and the University of Missouri System Interdisciplinary Intercampus Research Program.

REFERENCES

- [1] Wech, T., Lemke, A., and Medway, D., "Accelerating Cine-MR Imaging in Mouse Hearts Using Compressed Sensing," *Journal of Magnetic Resonance Imaging* **34**(5), 1072-1079 (2011).
- [2] Lustig, M., Donoho, D. L., and Pauly, J.M., "Sparse MRI: The Application of Compressed Sensing for Rapid MR Imaging," *Magnetic Resonance in Medicine* **58**, 1182 – 1195 (2007).
- [3] Hirst, B., Zheng, Y., Yang, M., and Ma, I., "3D spatio-temporal analysis for compressive sensing in magnetic resonance imaging of the murine cardiac cycle," *SPIE Digital Library* (2012).
- [4] Wang, Z., Bovik, A., Sheikh, H., and Simoncelli, E., "Image Quality Assessment: From Error Visibility to Structural Similarity," *IEEE Transactions on Image Processing* **13**, 600-612 (2004).
- [5] Han, S., Paulsen, J., Zhu, G., Song, Y., Chun, S., Cho, G., Ackerstaff, E., Koutcher, J., Cho, HyungJoon., "Temporal/spatial resolution improvement of in vivo DCE-MRI with compressed sensing-optimized FLASH," *Magnetic Resonance Imaging* **30**, 741 – 752 (2012)
- [6] Akcakaya, M., Basha, T., Chan, R., Manning, W., Nezafat, R., "Accelerated Isotropic Sub-Millimeter Whole-Heart Coronary MRI: Compressed Sensing Versus Parallel Imaging," *Magnetic Resonance in Medicine* (2013).